Environmental Science Nano

Surface Functionalized Nanoscale Metal Oxides for Arsenic (V), Chromium (VI), and Uranium (VI) Sorption: Considering Single- and Multi-Sorbate Dynamics

Journal:	*Environmental Science: Nano*
Manuscript ID	EN-ART-07-2020-000728.R1
Article Type:	Paper

Surface Functionalized Nanoscale Metal Oxides for Arsenic (V), Chromium (VI), and Uranium (VI) Sorption: Considering Single- and Multi-Sorbate Dynamics

Changwoo Kim[a], Seung Soo Lee[b], Kit Tan Kwan[c], Junseok Lee [a], Wenlu Li[a], Brandon J. Lafferty[d], Daniel E. Giammar[b], and John D. Fortner [a,*]

a Department of Chemical and Environmental Engineering, Yale University, New Haven, CT, 06520, United States
b Department of Energy, Environmental, and Chemical Engineering, Washington University, St. Louis, MO63130
c Department of Civil and Environmental Engineering, The Hong Kong University of Science & Technology, Clear Water Bay, Kowloon, Hong Kong
d U.S. Army Corps of Engineers, Engineer Research and Development Center, Vicksburg, MS, 39180, United States

*Corresponding author: john.fortner@yale.edu

Environmental Significance Statement

Heavy metal and metalloid separation and sensing in the environment remains a critical global challenge for environmental health, security, and energy disciplines, among others. For this, inorganic-organic nanoscale materials have gained significant interest as tunable, next generation, sorbents for contaminant separation. However, the vast majority of these studies have focused on single sorbate scenarios. In this study, we systematically compare a rationally designed set of inorganic-organic nanomaterials for single- and multi-sorbate systems, exploring arsenic, chromium, and uranium – with the goal of explicitly evaluating and elucidating competitive and/or cooperative effects when two or more contaminants are involved. Evaluation of sorption preferences (competitive/cooperative effects) were considered over an environmentally relevant range of water chemistries. Results clearly demonstrate the critical dynamics for multiple contaminant systems when considering sorption-based, nano-enhanced treatment technologies.

Journal Name

ARTICLE

Surface Functionalized Nanoscale Metal Oxides for Arsenic (V), Chromium (VI), and Uranium (VI) Sorption: Considering Single- and Multi-Sorbate Dynamics

Received 00th January 20xx,
Accepted 00th January 20xx

DOI: 10.1039/x0xx00000x

www.rsc.org/

Changwoo Kim,[a] Seung Soo Lee,[b] Kit Tan Kwan,[c] Junseok Lee,[a] Wenlu Li,[a] Brandon J. Lafferty,[d] Daniel E. Giammar,[b] and John D. Fortner[a,*]

Surface-functionalized Mn-Fe oxide nanocrystals (NCs) were evaluated for single- and multi-sorbate scenarios considering As(V), Cr(VI), and U(VI) in varied water chemistries (deionized (DI), ground, and sea water) at the same solution pH (pH 7.0). Multi-sorbate scenarios were further examined for competitive and/or cooperative effects. Precisely synthesized manganese ferrite ($MnFe_2O_4$) NCs were compared with iron oxide (Fe_3O_4) and manganese oxide (Mn_xO_y) nanocrystal cores in terms of soprtion capacities and colloidal stabliities. Positively charged cetyltrimethylammonium bromide (CTAB) and negatively charged oleyl phosphate (OP) were evaluted and compared as organic coating agents. $MnFe_2O_4$ NCs exhibited both enhanced sorption performance and colloidal stability compared with Fe_3O_4 and Mn_xO_y cores when functionalized with the same surfactant coatings. For $MnFe_2O_4$ NCs, maximum sorption of As(V), Cr(VI), and U(VI) was reached to 2.62, 3.43, and 4.27 mmol g^{-1} in DI water, respectively. Relative sorption capacity enhancement (compared with Fe_3O_4 and Mn_xO_y) is due to increased surface grafting densities of $MnFe_2O_4$ NCs, providing a larger number of sorption sites (functional group) for target sorbates and higher repulsive energy (osmotic and elastic-steric interaction) for increased stability. For As(V) and Cr(VI) multi-sorbate systems, all materials evaluated preferentially adsorbed As(V) over Cr(VI). This preference was further investigated and observed using a novel quartz crystal microbalance (QCM) technique.

Introduction

Elevated aqueous metal and metalloid concentrations in water require treatment due to regulatory requirements and related toxicity concerns.[1, 2] Further, hazardous metals and metalloids are globally distributed and often occur as mixed (i.e. multi-contaminant) systems.[3-5] For example, As(V) and Cr(VI) simultaneously occur in the case of chromated copper arsenate (CCA), which was historically used as an antimicrobial preservative (e.g. utility poles, fence, and playground equipment, etc.) to prevent fungal and bacterial decay.[6, 7] CCA leaching has been demonstrated as a source of contamination, which can be accelerated at low pH and elevated temperatures.[7-9] While CCA is now prohibited in the U.S. due to its toxicity, CCA treated equipment and furniture remain.[10] Another example is uranium ore, which can contain 1.2 to 10 weight percent of arsenic, typically as a uranyl arsenate mineral, leading to multi-contaminant scenarios.[11, 12]

Sorption and separation technologies are effective approaches for removing dissolved metals and metalloids from water. Towards this, sorption processes can be improved through incorporation of engineered, nanoscale materials, which provide large surface areas and high, or even unique, reactivities for target contaminants.[13-15] Looking forward, organic-inorganic hybrid nanocomposites have been considered as next generation nanoscale sorbents as they offer a controllable, rigid inorganic body, which is often functional (e.g. magnetic), and a flexible organic coating with tunable functional groups.[16-18] For example, the affinity for heavy metal contaminants (e.g. Pb, Cu, Hg, Ag, Cd, Co, and Ti) is described by Warner et al. for a series of organic-coated magnetite nanoscale crystals.[19] For enhanced sorption and removal of As(V) or Cr(VI), net positively charged organic ligands, including polyethylenimine (PEI), ethylenediamine, polyaniline, and chitosan, among others, have been evaluated.[20-23] Previous reports by this group demonstrated that surface-based surfactants with positively charged functional groups (e.g. cetyltrimethylammonium bromide (CTAB) and PEI) have excellent sorption performance for As(V) and Cr(VI).[24] In addition, negative phosphate functional groups, such as tributyl phosphate,[25, 26] oleyl phosphate (OP),[27, 28] sodium monododecyl phosphate (SDP),[29] disodium phosphate, and monopotassium phosphate[30] have shown high U(VI) affinity. While many of the aforementioned materials demonstrate excellent sorption properties for single sorbates, few have been evaluated for multi-sorbate scenarios.

[a] Department of Chemical and Environmental Engineering
Yale University
New Haven, CT 06520, United States
*corresponding author: john.fortner@yale.edu
[b] Department of Energy, Environmental, and Chemical Engineering
Washington University in St. Louis
St. Louis, MO 63130, United States
[c] Department of Civil and Environmental Engineering
The Hong Kong University of Science & Technology
Clear Water Bay, Kowloon, Hong Kong
[d] Engineer Research and Development Center
U.S. Army Corps of Engineers
Vicksburg, MS 39180, United States

† Electronic Supplementary Information (ESI) available:
See DOI: 10.1039/x0xx00000x

Here, the objective of this study was to evaluate and compare single- and multi-sorbate systems with a focus on competitive and/or cooperative effects in a range of water chemistries for a rationally designed matrix of organic-functionalized, metal oxide nanoscale sorbents. For this, we synthesized monodispersed manganese ferrite ($MnFe_2O_4$), iron oxide (Fe_3O_4), and manganese oxide (Mn_xO_y) NCs with CTAB and OP. NC sorption performance for single- and multi-sorbate scenarios, considering As(V), Cr(VI), and U(VI) under environmental relevant conditions (synthesized ground and sea waters) are presented. Additionally, specific multi-sorbate scenarios for As(V) and Cr(VI) were evaluated via batch and quartz crystal microbalance studies.

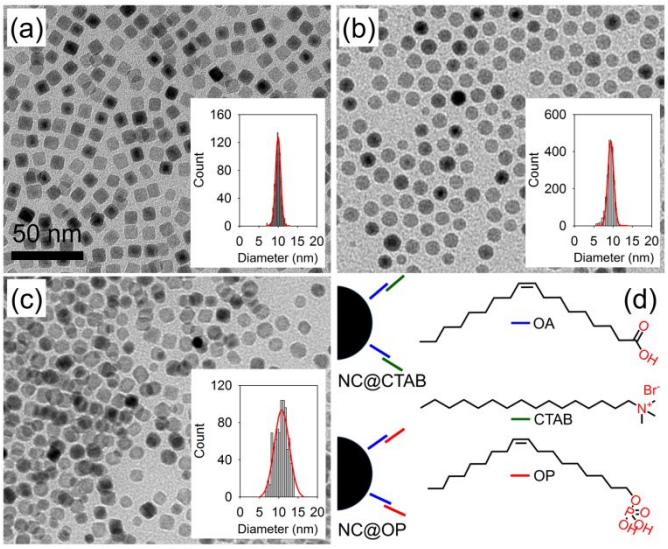

Fig. 1. TEM images of monodisperse metal oxide NCs (a) manganese ferrites, (b) iron oxide, and (c) manganese oxide. The inset Figure presents the histograms of the size distribution of NCs. (d) Schematic diagram of NCs and organic coatings. The average diameter and its standard deviation were 10.0 ± 0.7, 9.3 ± 0.9, and 10.6 ± 1.6 nm, respectively.

Results and Discussion

Synthesis and Characterization of Metal Oxide Nanocrystals

Three metal oxide (manganese ferrite, iron oxide, and manganese oxide) nanocrystals (NCs) were precisely synthesized by decomposition of Fe-oleate and/or Mn-oleate precursors in the presence of excess oleic acid at high temperature (320°C).[27, 31, 32] As synthesized, NCs are monodisperse in a non-polar solvent (hexane).[27, 33] TEM micrographs for as-synthesized NCs, along with size distributions, are presented in Figure 1. Manganese ferrites, iron oxide, and manganese oxide NCs were 10.0 ± 0.7, 9.3 ± 0.9, and 10.6 ± 1.6 nm, respectively. As reported previously,[27, 28, 33, 34] crystalline structures of the synthesized manganese iron oxide and iron oxide NCs match $MnFe_2O_4$ (JCPDS Card # 380430) and Fe_3O_4 (JCPDS Card # 190629), respectively. Manganese oxide NCs matched both MnO (JCPDS Card # 070230) and Mn_3O_4 (JCPDS Card # 240734), which has been previously reported for MnO core materials with a Mn_3O_4 shell (Fig. S1a†).[31, 33]

Synthesized metal oxide NCs were phase transferred from organic solvent into water through ligand encapsulation methods using cetyltrimethylammonium bromide (CTAB) and oleyl phosphate (OP).[24, 27] As(V) and Cr(VI) largely exist as anions over the wide pH range (i.e. above pH 2.2), while U(VI) can be cationic, neutral, and anionic depending on the aquatic chemistry (e.g. pH, presence of carbonates and organic ligands).[12] Positively charged CTAB is a favorable coating material for As(V) and Cr(VI), while OP having negative phosphate functional group, has been demonstrated to be favorable for U(VI) sorption.[24, 27] Once transferred into water, NCs were characterized by dynamic light scattering (DLS) at pH 7.0 to measure hydrodynamic diameter (D_H) and zeta potential (ζ). As shown in Fig. S1b†, D_H values for CTAB functionalized manganese ferrite ($MnFe_2O_4$@CTAB), magnetite (Fe_3O_4@CTAB), and manganese oxide (Mn_xO_y@CTAB) NCs were 22.7, 24.1, and 23.4 nm, respectively. D_H of OP coated manganese ferrite ($MnFe_2O_4$@OP), magnetite (Fe_3O_4@OP), and manganese oxide (Mn_xO_y@OP) NCs were 22.3, 25.2, and 21.9 nm, respectively. ζ values of the NCs were 23.7, 23.4, and 25.6 mV, for $MnFe_2O_4$@CTAB, Fe_3O_4@CTAB, and Mn_xO_y@CTAB, respectively and -27.7, -27.3, and -26.3 mV, respectively for $MnFe_2O_4$@OP, Fe_3O_4@OP, and Mn_xO_y@OP (Fig. S1c†). Surfactant loadings on $MnFe_2O_4$@CTAB, Fe_3O_4@CTAB, and Mn_xO_y@CTAB were ca. 16,000, 5,000, and 3,000 molecules per NC, respectively (Fig. S1d†). The number of OP per NC were 19,000, 7,000, and 4,000 for $MnFe_2O_4$@OP, Fe_3O_4@OP, and Mn_xO_y@OP, respectively. Interestingly, surfactant loading by both CTAB and OP was highest for $MnFe_2O_4$ followed by Fe_3O_4 and Mn_xO_y, though surface areas of all NPs are similar. Increased surface coatings such as CTAB and OP, also enhance aqueous stability, by lowering interfacial surface energies.[35]

As(V), Cr(VI), and U(VI) Sorption in Single-Sorbate Systems

Colloidal stability is crucial for sorption performance via conservation of favorable surface sites. Before evaluating specific sorption performance of synthesized NCs, aqueous stabilities were described by their critical coagulation concentration (CCC). As shown in Fig. S2a†, CCC values for Mn_xO_y@CTAB are 259 mM in NaCl and 133 mM in $CaCl_2$. As the functional head group of CTAB is a positively charged quaternary ammonium, the divalent cation Ca^{2+} influences NCs as co-ions. $MnFe_2O_4$@CTAB and Fe_3O_4@CTAB were colloidally stable under high mono- or di-valent cation concentrations, maintaining their initial diameter in 1 M NaCl and up to 1M $CaCl_2$. As presented in Fig. S2b, c, and d†, CCC values for OP coated NCs were 450, 695, and 1130 mM in NaCl and 6.9, 7.1, and 9.9 mM in $CaCl_2$ for Mn_xO_y, Fe_3O_4, and $MnFe_2O_4$ NCs, respectively. Divalent counter ions (Ca^{2+}) have a strong effect on colloidal stability of the OP coated NCs, as they have a negatively charged phosphate head group. We also observed that NCs with higher grafting density (e.g. $MnFe_2O_4$) have higher colloidal stability indicating that surface grafting density plays a critical role in colloidal stability by underpinning repulsive energies, including elastic-steric, osmotic, and electrostatic repulsion.[36-39]

Sorption performance was first explored for single-sorbate systems in DI water at pH 7.0 ± 0.2. For these, we observe consistent Langmuirian behavior, for all conditions evaluated, compared to Freundlich model fits. Such a result is not surprising, as these materials have finite coatings with identical functional groups (amine or phosphate), which are equally available. As expected, positively (oppositely) charged CTAB functionalized NCs ($MnFe_2O_4$@CTAB, Fe_3O_4@CTAB, and Mn_xO_y@CTAB) showed higher As(V) and Cr(VI) sorption performance than negatively charged OP coated NCs ($MnFe_2O_4$@OP, Fe_3O_4@OP, and Mn_xO_y@OP) (Fig.2a and b). The maximum sorption density (q_{max}) of CTAB stabilized NCs for As(V) was 2.62 ± 0.15, 0.86 ± 0.02, and 0.31 ± 0.03 mmol g^{-1} for $MnFe_2O_4$, Fe_3O_4,

and Mn_xO_y, respectively and q_{max} of OP functionalized NCs towards As(V) was 0.97 ± 0.03, 0.14 ± 0.02, and 0.06 ± 0.01 mmol g^{-1} for $MnFe_2O_4$, Fe_3O_4, and Mn_xO_y, respectively. The q_{max} of CTAB stabilized NCs for Cr(VI) was 3.43 ± 0.19, 2.53 ± 0.01, and 0.45 ± 0.02 mmol g^{-1} for $MnFe_2O_4$, Fe_3O_4, and Mn_xO_y, respectively and q_{max} of OP functionalized NCs towards Cr(VI) was 1.39 ± 0.09, 0.20 ± 0.03, and 0.09 ± 0.01 mmol g^{-1} for $MnFe_2O_4$, Fe_3O_4, and Mn_xO_y, respectively. We hypothesize that positively charged quaternary amine group of CTAB is the key binding sites for both As(V) and Cr(VI), as they exist in an anionic form above pH ca. 2.2.[24] For U(VI) removal, negatively charged OP functionalized NCs showed outstanding sorption performance (Fig. 2c), as observed by this lab and others.[27] The q_{max} towards U(VI) for OP coated NCs was 4.27 ± 0.38, 2.47 ± 0.13, and 1.91 ± 0.08 mmol g^{-1} NCs for $MnFe_2O_4$, Fe_3O_4, and Mn_xO_y, respectively. In comparison, the q_{max} towards U(VI) for CTAB functionalized NCs was 0.65 ± 0.08, 0.64 ± 0.05, and 0.69 ± 0.04 mmol g^{-1} NCs for $MnFe_2O_4$, Fe_3O_4, and Mn_xO_y, respectively. Additionally, we normalized sorption to the number of (coating) functional groups in Table S1. As expected, U sorption capacity per number of phosphate groups decreases with increasing the surfactant grafting density. This is likely due to increased steric hindrance for higher surfactant loadings for a relatively large ion.[24, 40]

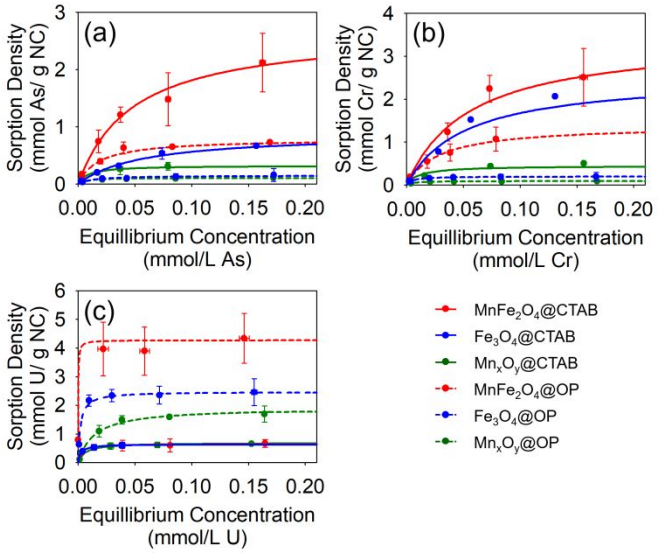

Fig. 2. (a) As(V), (b) Cr(VI), and (c) U(VI) sorption isotherm on metal oxide ($MnFe_2O_4$ (red), Fe_3O_4 (blue), and Mn_xO_y (green)) NCs coated with the positively charged surface stabilizer (CTAB (solid line)) or the negatively charged organic coating (OP (dotted line)). Experiments were conducted in DI water at pH 7.0 ± 0.2. Dot plots with error bars and line plots present experiment measurement values with standard deviations and Langmuir isotherm fittings, respectively.

In a previous report, we observed that organic coated $MnFe_2O_4$ readily adsorb U(VI) as part of an expanded series of particle core compositions evaluated ($MnFe_2O_4$, Fe_3O_4, and Mn_xO_y).[27] Further, we verified $MnFe_2O_4$ NCs had enhanced (surface) reduction potentials compared to the Fe_3O_4, and Mn_xO_y NCs.[27] Here, we also observe that $MnFe_2O_4$ NCs have the highest grafting density, comparatively, which is key for sorption sites and stability. Two obvious reasons for these differences include: 1) the high colloidal stability of $MnFe_2O_4$ NCs in water compared to the Fe_3O_4 and Mn_xO_y NCs (Fig. S2 and S3†), and 2) the highest loading of organic surface coatings with specific functional groups (CTAB and OP) on the surface of $MnFe_2O_4$ NCs increased sorption capacity – i.e. a relative increase in favorable surface sites.

Effects of Water Chemistry on Single-Sorbate Systems

To understand how environmentally relevant ionic conditions affect sorption processes, we considered DI water, synthesized ground water, and synthesized sea water at pH 7.0 ± 0.2 using $MnFe_2O_4$@CTAB for As(V) and Cr(VI) and $MnFe_2O_4$@OP for U(VI). The composition of the synthesized ground water and sea water are presented in Table S2.[41, 42] Carbonates were not controlled in these sorption systems. The impact of the carbonate system on As(V) and Cr(VI) species in water is negligible, but carbonates are important in U(VI) species due to the formation of uranyl carbonate with various hydrated complexes.[43] As presented in Fig. 3, sorption capacities for As(V) and U(VI) decreased in ground water and sea water conditions. The q_{max} towards As(V) was 2.62 ± 0.15, 0.57 ± 0.08, and, 0.34 ± 0.05 mmol g^{-1} for DI, ground water, and, sea water, respectively and q_{max} towards U(VI) was 4.27 ± 0.38, 2.21 ± 0.05, and, 1.00 ± 0.03 mmol g^{-1} for DI, ground water, and, sea water, respectively. The Cr(VI) sorption density for $MnFe_2O_4$@CTAB was dramatically reduced in the ground and sea water conditions.[44] The q_{max} towards Cr(VI) was 3.43 ± 0.19, 0.05 ±0.01, and, 0.00 ± 0.00 mmol g^{-1} for DI, ground water, and sea water, respectively. The surface area of $MnFe_2O_4$ did not play a critical role in ionic conditions dependent sorption performance as NCs maintained their initial size after sorption isotherm test, except for the case of U(VI) sorption in synthesized sea water (Fig. S4†).

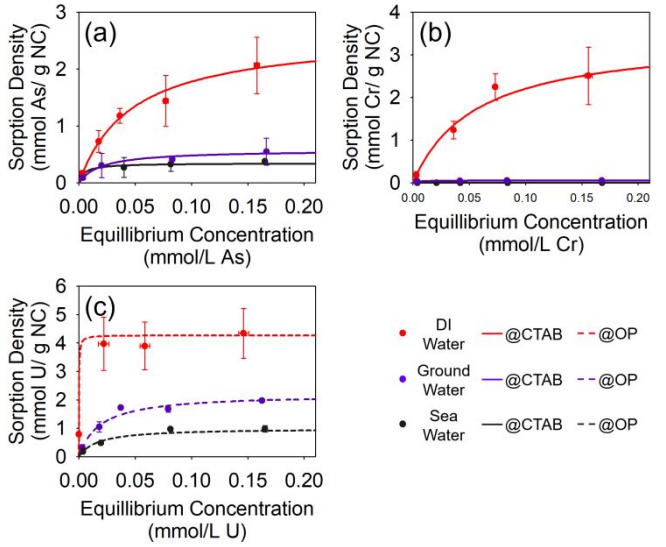

Fig. 3. (a) As(V) and (b) Cr(VI) sorption isotherm on manganese ferrite ($MnFe_2O_4$) NCs coated with CTAB (solid line) and (c) U(VI) sorption isotherm on $MnFe_2O_4$ with OP (dotted line) in DI water (red), synthesized ground water (purple), and sea water (black). Every sorption isotherm was obtained at pH 7.0 ± 0.2.

To further understand sorption affinities under real world waters, sorption densities were explored using each major divalent cation and divalent anion of the synthesized ground and sea water (Mg^{2+}, Ca^{2+}, and SO_4^{2-}). To clearly observe competitive effects, we selected the highest initial sorbate concentration (0.168 mM). In addition, effects of total ionic strength of ground water and sea water were evaluated using monovalent ions (NaCl). For this, we evaluated As(V) and Cr(VI) sorption experiments using $MnFe_2O_4$@CTAB, and U(VI) sorption using $MnFe_2O_4$@OP at pH 7.0 ±0.2 over seven ionic conditions. The type and concentration of ions considered are as follow; 45.2 mM $MgCl_2$, 8.6 mM $CaCl_2$, 27.9 mM Na_2SO_4, and 694.6

mM NaCl for sea water condition and 0.8 mM $CaCl_2$, 1.0 mM Na_2SO_4, and 10.6 mM NaCl for ground water condition. We calculated a normalized sorption density by dividing sorption densities by those in DI water.

As shown in Fig. 4a, total ionic strength is not a significant factor in As(V) sorption performance. Normalized sorption densities (described as a fraction of sorption density in D.I. water) for total ionic strength of ground water (10.6 mM NaCl) and sea water (694.6 mM NaCl) were 0.84 and 0.98, respectively. For Cr(VI) sorption, both ground water and sea water significantly affected Cr(VI) sorption (Fig. 4b). Normalized sorption densities were observed to be 0.30 (10.6 mM NaCl) and 0.00 (694.6 mM NaCl). Divalent cations (Mg^{2+} and Ca^{2+}) have a significant effect on Cr(VI) sorption density with normalized sorption densities of 0.0 (45.2 mM $MgCl_2$), 0.15 (8.6 mM $CaCl_2$), and 0.64 (0.8 mM $CaCl_2$). Ionic strength influences double layer thickness of $MnFe_2O_4$@CTAB,[45] thus affecting binding for both As(V) and Cr(VI). In the presence of sulfate ions (SO_4^{2-}), As(V) and Cr(VI) sorption performance for $MnFe_2O_4$@CTAB was significantly hindered; normalized sorption densities were 0.18 (27.9 mM Na_2SO_4) and 0.26 (1.0 mM Na_2SO_4) for As(V), and 0.00 (27.9 mM Na_2SO_4) and 0.02 (1.0 mM Na_2SO_4) for Cr(VI). Also, phosphate, even at low concentrations, has been widely observed to be competitive with A(V) and Cr(VI) sorption.[46] Taken together, we conclude that divalent anions, act as effective competing ions for both As(V) and Cr(VI). Contrary to As(V) and Cr(VI), sulfate ions did not have a significant effect on the U(VI) sorption performance on $MnFe_2O_4$@OP (Fig. 4c). Normalized sorption density above 0.8 was observed in presence of sulfate ions. However, normalized sorption density was observed to be 0.27 (45.2 mM $MgCl_2$), 0.26 (8.6 mM $CaCl_2$), and 0.67 (0.8 mM $CaCl_2$) in presence of divalent cations, such as Mg^{2+} and Ca^{2+}. With increasing ionic strength, normalized U(VI) sorption density also decreased to 0.53 in ground water and 0.20 in sea water due to charge screening.[27]

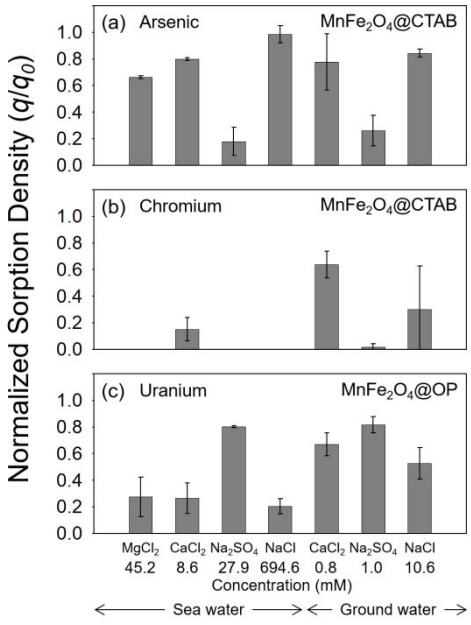

Fig. 4. Normalized (a) As(V), (b) Cr(VI), and (c) U(VI) sorption density on $MnFe_2O_4$@OP or $MnFe_2O_4$@CTAB with a series of ions and concentrations. The 694.6 mM NaCl concentration is adjusted to the total ionic strength of sea water. The 10.6 mM NaCl concentration is adjusted to the total ionic strength of ground water. Error bars present standard deviations. Every test was performed at pH 7.0 ± 0.2.

Multi-Sorbate Systems

Multi-sorbate systems were explored to evaluate competitive and/or cooperative effects when two or more sorbates are present. Manganese ferrite ($MnFe_2O_4$) NCs, which showed outstanding sorption performance in single-sorbate systems, were used for multi-contaminant sorption studies. For this, four different systems were explored: As(V) and Cr(VI); As(V) and U(VI); Cr(VI) and U(VI); and As(V), Cr(VI), and U(VI). For As(V) and U(VI) systems, isotherm results are complicated by the fact that As(V) and U(VI) readily formed uranyl arsenate precipitates.[11] For other combinations, As(V) and Cr(VI) showed significant competitive effects, which is further explored here. Other multi-sorbate systems (Cr(VI) and U(VI); As(V), Cr(VI), and U(VI)) are presented in ESI (Fig. S5†).

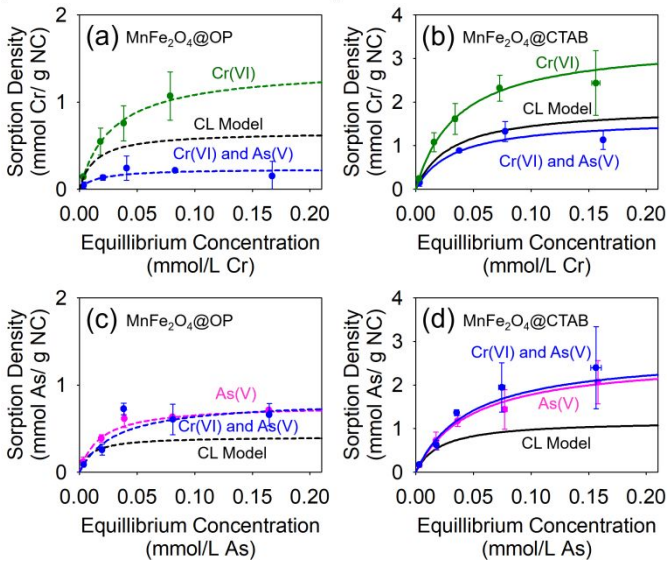

Fig. 5. Single- and multi-sorption isotherm on $MnFe_2O_4$ NCs coated with CTAB (solid line) or OP (dotted line); single-sorbate systems (As(V) (pink) and Cr(VI) (green)) and multi-sorbate systems (As(V) and Cr(VI) (blue)). Experiments were conducted in DI water at pH 7.0 ± 0.2. Black solid and dotted line presents the competitive Langmuir isotherm (CL) model.

As(V) and Cr(VI) Multi-Sorbate System

Cr(VI) sorption isotherms for dual-sorbate scenarios (as As(V) and Cr(VI)) and single-sorbate systems for $MnFe_2O_4$@OP and $MnFe_2O_4$@CTAB are presented in Fig. 5a and b. Cr(VI) sorption on $MnFe_2O_4$@OP was significantly hindered in the presence of As(V); the q_{max} for Cr(VI) was 1.39 ± 0.09 mmol g^{-1} for the single Cr(VI) system and the q_{max} for multi-sorbate systems was below 0.23 ± 0.04 mmol g^{-1}. Cr(VI) sorption performance of $MnFe_2O_4$@CTAB was also significantly decreased in the presence of As (V); the q_{max} for Cr(VI) was 3.43 ± 0.19 mmol g^{-1} for the single-sorbate system and 1.62 ± 0.08 mmol g^{-1} in the presence of As(V). Regardless of coating, Cr(VI) sorption capacity was greatly reduced in the presence of As(V) due to preferred sorption.[47] We further explored Cr(VI) sorption isotherms via a classic competitive Langmuir (CL) model, which was derived from the same assumption as the original Langmuir isotherm.[48] For both $MnFe_2O_4$@OP and $MnFe_2O_4$@CTAB, measured Cr(VI) sorption was lower than that calculated by the CL model. In the CL model, charge neutralization via competitive ions (here As(V)) is not considered. We speculate that decrease of electrostatic affinity is possible reason for reduction of Cr(VI) sorption in As(V) and

Cr(VI) multi-sorbate system. In the case of As(V) sorption, measured sorption density was higher than modeled density; 2.72 ± 0.22 and 2.62 ± 0.15 mmol g^{-1} for $MnFe_2O_4$@CTAB with and without Cr(VI), respectively and 0.96 ± 0.05 and 0.97 ± 0.03 mmol g^{-1} for $MnFe_2O_4$@OP with and without Cr(VI), respectively (Fig. 5c and d). Within one standard deviation of the q_{max} values, the presence of Cr(VI)had no influence on As(V) sorption performance. It is therefore likely that electrostatic attraction is not a governing mechanism for Cr(VI) sorption.

Previous reports have explored and demonstrated As(V) and Cr(VI) sorption preference for different interfaces. For example, metal (hydr)oxides can exhibit sorption preference toward As(V) over Cr(VI) due to strong inner-sphere complexes (between As(V) and metal (hydr)oxides).[49] Negatively charged sorbents, including carbonaceous nanofibers, and pine bark (composed of lignin, cellulose, and hemi-cellulose) have shown Cr(VI) sorption preference.[50, 51] Further, previous studies report a slight Cr(VI) sorption preference for anion exchange sorbents containing cationic organic polymers.[49] Here, positively charged $MnFe_2O_4$@CTAB displays excellent capacity for both As(V) and Cr(VI), with As(V) preferred.

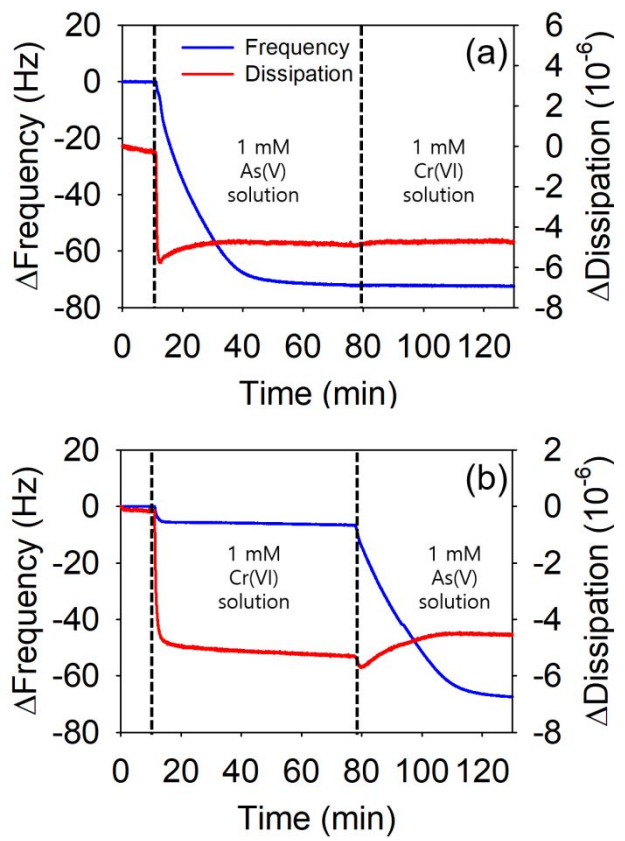

Fig. 6. Time dependent frequency and dissipation shift (overtone n = 3) of the PDDA coated Q-sensor. At 10 min, (a) 1 mM As(V) solution or (b) 1 mM Cr(VI) solution were applied to the Q-sensor. Then at 77 min, after frequency and dissipation signals were stabilized, (a) 1 mM Cr(VI) solution and (b) 1mM As(V) solution were flowed to the Q-sensors.

To further quantify sorption preference as a function of organic coating between As(V) and Cr(VI), real time sorption behavior was investigated via quartz crystal microbalance with dissipation (QCM-D). To mimic the quaternary amine group (functional head group of CTAB), quaternary amine polymer poly(diallyldimethylammonium chloride) (PDDA) was grafted on the surface of the silica Q-sensor by "grafting to" method;[52] PDDA was anchored from the PDDA solution (2.0 wt.% in H_2O) to the Q-sensor surface (Fig. S6†). It is recognized that potential changes in polymer configuration may affect a Sauerbrey relationship.[53, 54] However, if all other variables are held constant, as done here, we can confirm PDDA polymer interaction dynamics with As(V) and Cr(VI) via real time frequency and dissipation shifts.

To verify the As(V) and Cr(VI) sorption preference, we flowed either As(V) or Cr(VI) solutions (1 mM) at pH 7 over the PDDA coated sensor. As shown in Fig. 6, frequency and dissipation of PDDA coated Q-sensor significantly decreased after applying 1 mM As(V) solution. In the Cr(VI) solution, a similar dissipation decrease was observed with a small(er) frequency decrease. After signal stabilization, indicating equilibrium, we switched the influent solution from As(V) to Cr(VI) and Cr(VI) to As(V), respectively. As(V) bound to PDDA coated Q-sensor had no significant frequency and dissipation change upon the addition of 1 mM Cr(VI) solution. In contrast, for Cr(VI) sorbed onto PDDA, frequency and dissipation shift where obvious when As(VI) solution was introduced, indicating a facile surface exchange. This observation provides clear evidence for As(V) sorption preference over Cr(VI) for amine-based functional groups.

Conclusions

Composition varied manganese-iron oxide NCs were synthesized and surface functionalized with CTAB and OP to explore their sorption performance on single- and multi-sorbate systems considering As(V), Cr(VI), and U(VI). The results obtained in this work clearly demonstrate that functional groups of organic coating(s) provide not only specific affinity to a single-sorbate (As(V), Cr(VI), and U(VI)), but also colloidal stability for core metal oxide. For the As(V) and Cr(VI) multi-sorbate system, we observed that surface coating (i.e. CTAB) had As(V) sorption preference over Cr(VI). For practical application(s) of advanced nanoscale sorbents such as these, the effects of pH, presence of other ions, and separation processes should be further investigated.

Experimental

Materials.

Chemical materials including iron(III) chloride hexahydrate ($FeCl_3 \cdot 6H_2O$, 97%), manganese(II) chloride tetrahydrate ($MnCl_2 \cdot 4H_2O$, 99.99%), oleic acid (OA, technical grade, 90%), 1-octadecene (ODE, technical grade, 90%), cetyltrimethylammonium bromide (CTAB, 95%), ethanol (99.9%), acetone (99.5%), hexane (98.5%), sodium arsenate ($Na_2HAsO_4 7H_2O$), potassium chromate ($K_2Cr_2O_7$), and poly(diallyldimethylammonium chloride) were purchased from Sigma-Aldrich. Oleyl phosphate (OP) and sodium oleate (97%) were obtained from TCI America. Uranyl nitrate hexahydrate ($UO_2(NO_3)_2 \cdot 6H_2O$) was purchased from Antec, Inc.

Synthesis of Iron Oleate and Manganese Oleate.

Iron oleate (Fe-oleate) and manganese oleate (Mn-oleate) were synthesized by the method reported by An et al.[55] Fe-oleate was synthesized by heating the mixture of iron (III) chloride hexahydrate (40 mmol) and oleic acid (120 mmol) in ethanol (100 g), water (50 g), and hexane (80 g) for 4 h at 58°C. The mixture of manganese chloride

tetrahydrate (40 mmol) and oleic acid (80 mmol) in ethanol (100 g), water (50 g), and hexane (80 g) were heated 4 h at 58°C for Mn-oleate synthesis. The resulting metal-oleate (Fe-oleate or Mn-oleate) suspensions were purified over six times using water and ethanol (1:1 volume ratio) and then the purified metal-oleate was extracted using hexane.

Synthesis of Manganese Ferrite, Iron Oxide, and Manganese Oxide Nanocrystals.

Manganese ferrite, iron oxide, and manganese oxide nanocrystals (NCs) were synthesized by the method reported by our previous reasearch.[27] Iron oxide NCs were synthesized by decomposition of Fe-oleate (0.31 mmol) with oleic acid (0.21 mmol) in 1-octadecene (5 g) at 320°C for 1 h. Manganese oxide NCs were synthesized by Mn-oleate decomposition at 320°C; Mn-oleate (0.3 mmol) with oleic acid (0.15 mmol) was used for synthesizing NCs in 1-octadecene (5 g) as a solvent. Manganese ferrite NCs were synthesized by decomposition of the mixture of metal-oleate as precursors (Mn-oleate (0.27 mmol) and Fe-oleate (0.54 mmol)) with oleic acid (2 mmol) in 1-octadecene (5 g) at 320°C for 1 h. All NCs were synthesized under argon purging (99.999%). The resulting NCs were washed with ethanol (20 mL) and acetone (25 mL); the purify process was repeated over six times. The purified NCs were stored in the non-polar solvent hexane.

Surface Functionalization and Phase Transfer.

Synthesized NCs were organically surface functionalized and phase transferred from the organic solvent (hexane) to water phase by ligand encapsulation method.[56, 57] CTAB and OP were used as phase transfer agents. Particular amounts of surface stabilizer (1 to 10 mmol) were mixed with 0.5 mL nanocrystal (NC) in hexane (particle number of 3.8×10^{17}) and vigorously stirred in 8 mL DI water (>18.2 MΩ-cm resistivity, Milli-Q, Millipore Corp). The mixture of phase transfer agents and NCs was probe-sonicated (Qsonica, Q-700, Taperd microtip) for 5 to 10 min at 80% amplitude with full cycle. The phase transferred NC (in water) was put in the fume hood for over 24 h to evaporate excess hexane and then purified using a stirred cell with an ultra-filtration membrane (cellulose, 100K Dalton, Millipore) at 10 psi using argon gas. Lastly, the resulting solution was further filtrated by syringe filter (0.22 μm, WHATMAN-PTFE) and the concentration of the NC solution was measured using inductively coupled plasma optical emission spectroscopy (ICP-OES, Perkin Elmer Optima 7300 DV).

Sorption Isotherm.

The synthesized metal oxide NCs were used as sorbents for As(V), Cr(VI), and U(VI) over ranges of 0.021 to 0.168 mM at pH 7.0 ± 0.2. Every sorption isotherm was obtained at least duplicate. In the multi-sorption systems, all initial contaminant concentrations were the same as molar concentration. pH of the solution was adjusted using HNO_3 and NaOH solution before batch sorption experiments and during the sorption test (after 4 and 8 h). All experiments were closed systems except during pH adjustments. After 24 h, to measure the sorption isotherm, NCs were separated using ultracentrifugation (Sorvall WX Ultra 80, Thermo scientific) at 50,000 rpm for 2 h and supernatants were measured using inductively coupled plasma mass spectrometry (ICP-MS, Perkin Elmer ELAN DRC II). The calculated sorption isotherm was plotted by the Langmuir isotherm (equation 1).

$$q_e = \frac{q_{max} K_L C_e}{(1 + k_L \cdot C_e)} \quad (1)$$

Where q_e is the sorption density of the system (mmol as sorbed contaminants per g as NCs), q_{max} is maximum sorption density, K_L is Langmuir sorption constant (L mmol^{-1}), and C_e is the equilibrium concentration of contaminants (mmol L^{-1}). Every measured q_{max} and K_L were summarized in Table S3 and S4.

Competitive Langmuir Isotherm Model (CL model)

To describe the competitive adsorption, the CL model was used.[48] This model has same assumptions of the basic Langmuir model. It is assumed that the surface of adsorbent is uniform, adsorbed molecules are not interact, and all adsorption mechanism is same. As the $q_{max,a}$, we used a q_{max} from the single-sorbate isotherms (Table S2). The model equation is as follows (equation 2):

$$q_{e,a} = \frac{q_{max,a} K_{L,a} C_{e,a}}{(1 + k_{L,a} \cdot C_{e,a} + k_{L,b} \cdot C_{e,b})} \quad (2)$$

The parameters of CL model are drawn from the corresponding single Langmuir isotherm.

Critical Coagulation Concentration (CCC).

The critical coagulation concentration (CCC) of NCs was measured in varied concentrations of NaCl or $CaCl_2$ using the dynamic light scattering (DLS) method at pH 7.0. The attachment efficiency (α) of NCs was calculated by dividing the measured aggregation rate constant (k_{11}) into the fast aggregation rate constant ($k_{11,fast}$). Here, CCC is at a minimum concentration when the α becomes one (equation 3).

$$\alpha = \frac{k_{11}}{k_{11,fast}} \quad (3)$$

Transmission Electron Microscopy (TEM).

The diameter of synthesized NCs was measured using a transmission electron microscope (TEM, Tecnai G2 Spirit, FEI). TEM images were analyzed by Image Pro Plus 6.0 (Media Cybernetics, USA); size and size distribution were obtain by counting over a thousand of NCs.[58]

Hydrodynamic Diameter and Zeta Potential.

The hydrodynamic diameters and zeta potential of NCs were determined by dynamic light scattering method (Malvern, Zetasizer Nano ZS, ZEN3600) at 22°C.

X-Ray Diffraction (XRD).

XRD patterns (from 20° to 80° of 2θ) of synthesized NCs were measured using a powder diffractometer (Bruker d8 Advance X-ray Diffractometer) with Cu Kα radiation (1.54 Å).

Total Organic Carbon (TOC).

A total organic carbon analyzer (TOC, Shimadzu Scientific Instrument) was used to measure the number of organic molecules coated on NC.

Quartz Crystal Microbalance with Dissipation (QCM-D).

Quartz crystal microbalance with dissipation (QCM-D, Q-sense E4, Biolin Scientific) was used with a quartz sensor (5MHz silica coated QCM-D crystal, QSX-202, Q-sense) at 22.00 ± 0.02°C under 100 μL min^{-1} of flow rate (ISM935, ISMATEC) to verify the sorption preference. Real time frequency shifts obtained by QCM-D can be correlated with a variation of surface deposited mass based on the Sauerbrey relationship (equation 4).[59]

$$\Delta m = -\frac{C \Delta F_n}{n} \quad (4)$$

Here, m is the total deposited mass on the Q-sensor, C is the quartz sensor constant, F_n is the shift in resonance frequency, and n is the resonance number (1, 3, 5, 7, 11 and 13). Dissipation obtained by QCM-D presented viscoelastic properties of the adsorbed layer on the Q-sensor. The dissipation during the oscillation of Q-sensor is described below (equation 5).[54, 60]

$$D = \frac{E_d}{2\pi E_s} \quad (5)$$

Where, D is the energy dissipation, E_d is the energy dissipated during one oscillation, and E_s is the energy stored in the oscillation system.

Conflicts of interest

There are no conflicts to declare.

Acknowledgements

This work is supported by U.S. Army Corps of Engineers (W912HZ-13-2-0009-P00001) and the US National Science Foundation (CBET 1437820). XRD measurements were made possible by a grant from the U.S. National Science Foundation (EAR-1161543). TEM, DLS, Ultracentrifugation, ICP-OES, and ICP-MS were provided by the Nano Research Facility (NRF) at Washington University in St. Louis. The authors acknowledge Professor Cindy Mittanck for reviewing the manuscript.

Notes and references

† Electronic Supplementary Information (ESI) available: Supporting Information includes detailed descriptions for the hydrodynamic diameter of NCs after sorption isotherm, frequency and dissipation shifts for PDDA coating on Q-sensor, composition of synthesized ground water and sea water, summary of maximum sorption density and Langmuir constant. See DOI: 10.1039/x0xx00000x

References

1. L. Järup, *British medical bulletin*, 2003, **68**, 167-182.
2. D. G. Mazumder, *Indian Journal of Medical Research*, 2008, **128**, 436.
3. A. H. Welch, D. Westjohn, D. R. Helsel and R. B. Wanty, *Ground water*, 2000, **38**, 589-604.
4. J. Nolan and K. A. Weber, *Environmental Science & Technology Letters*, 2015, **2**, 215-220.
5. J. Guertin, J. A. Jacobs and C. P. Avakian, *Chromium (VI) handbook*, CRC press, 2016.
6. J. Hingston, C. Collins, R. Murphy and J. Lester, *Environmental Pollution*, 2001, **111**, 53-66.
7. A. H. Moghaddam and C. N. Mulligan, *Waste Management*, 2008, **28**, 628-637.
8. J. R. Jambeck, T. Townsend and H. Solo-Gabriele, *Journal of Hazardous Materials*, 2006, **135**, 21-31.
9. J. L. Taylor and P. A. Cooper, *Holzforschung*, 2005, **59**, 467-472.
10. A. Chini, R. Buck, S. Nakajima and M. Russell, *Barriers for Deconstruction and Reuse/Recycling of Construction Materials*, 2014, 115.
11. L. D. Troyer, Y. Tang and T. Borch, *Environmental science & technology*, 2014, **48**, 14326-14334.
12. R. M. Coyte and A. Vengosh, *Environmental Science & Technology*, 2020, **54**, 4367-4375.
13. M. R. Wiesner and J.-Y. Bottero, *Applications and Impacts of Nanomaterials*, 2007, 395-517.
14. J. Theron, J. A. Walker and T. E. Cloete, *Crit Rev Microbiol*, 2008, **34**, 43-69.
15. N. Savage and M. S. Diallo, *Journal of Nanoparticle Research*, 2005, **7**, 331-342.
16. M. E. Davis, C. Saldarriaga, C. Montes, J. Garces and C. Crowdert, *Nature*, 1988, **331**, 698-699.
17. P. B. Moore and J. Shen, 1983.
18. C. M. Wang, L. W. Lee, T. Y. Chang, Y. C. Chen, H. M. Lin, K. L. Lu and K. H. Lii, *Chemistry–A European Journal*, 2015, **21**, 1878-1881.
19. C. L. Warner, R. S. Addleman, A. D. Cinson, T. C. Droubay, M. H. Engelhard, M. A. Nash, W. Yantasee and M. G. Warner, *ChemSusChem*, 2010, **3**, 749-757.
20. T. Zhou, C. Li, H. Jin, Y. Lian and W. Han, *ACS applied materials & interfaces*, 2017, **9**, 6030-6043.
21. A. G. Yavuz, E. Dincturk-Atalay, A. Uygun, F. Gode and E. Aslan, *Desalination*, 2011, **279**, 325-331.
22. B. Liu and Y. Huang, *Journal of Materials Chemistry*, 2011, **21**, 17413-17418.
23. N. Kim, M. Park, Y.-S. Yun and D. Park, *Chemosphere*, 2019, **226**, 67-74.
24. C. Kim, S. S. Lee, B. J. Lafferty, D. Giammar and J. Fortner, *Environmental Science: Nano*, 2018, **5**, 556-563.
25. S. Mishra, J. Dwivedi, A. Kumar and N. Sankararamakrishnan, *New Journal of Chemistry*, 2016, **40**, 1213-1221.
26. X.-F. Yu, Y.-H. Liu, Z.-W. Zhou, G.-X. Xiong, X.-H. Cao, M. Li and Z.-B. Zhang, *Journal of Radioanalytical and Nuclear Chemistry*, 2014, **300**, 1235-1244.
27. S. S. Lee, W. Li, C. Kim, M. Cho, B. J. Lafferty and J. D. Fortner, *Journal of Materials Chemistry A*, 2015, **3**, 21930-21939.
28. C. Kim, S. S. Lee, B. J. Reinhart, M. Cho, B. J. Lafferty, W. Li and J. D. Fortner, *Environmental Science: Nano*, 2018, **5**, 2252-2256.
29. W. Li, L. D. Troyer, S. S. Lee, J. Wu, C. Kim, B. J. Lafferty, J. G. Catalano and J. D. Fortner, *ACS Applied Materials & Interfaces*, 2017, **9**, 13163-13172.
30. E. Calì, J. Qi, O. Preedy, S. Chen, D. Boldrin, W. Branford, L. Vandeperre and M. Ryan, *Journal of Materials Chemistry A*, 2018, **6**, 3063-3073.
31. K. An, M. Park, J. H. Yu, H. B. Na, N. Lee, J. Park, S. H. Choi, I. C. Song, W. K. Moon and T. Hyeon, *European Journal of Inorganic Chemistry*, 2012, **2012**, 2148-2155.
32. C. Kim, S. S. Lee, W. Li and J. D. Fortner, *Applied Catalysis A: General*, 2020, **589**, 117303.
33. S. S. Lee, W. Li, C. Kim, M. Cho, J. G. Catalano, B. J. Lafferty, P. Decuzzi and J. D. Fortner, *Environmental Science: Nano*, 2015, **2**, 500-508.
34. S. Sun, H. Zeng, D. B. Robinson, S. Raoux, P. M. Rice, S. X. Wang and G. Li, *Journal of the American Chemical Society*, 2004, **126**, 273-279.
35. L. Peltonen and J. Hirvonen, *Journal of Pharmacy and Pharmacology*, 2010, **62**, 1569-1579.
36. E. M. Hotze, T. Phenrat and G. V. Lowry, *Journal of environmental quality*, 2010, **39**, 1909-1924.

37. T. Phenrat, N. Saleh, K. Sirk, H.-J. Kim, R. D. Tilton and G. V. Lowry, *Journal of Nanoparticle Research*, 2008, **10**, 795-814.
38. J. Ortega-Vinuesa, A. Martın-Rodrıguez and R. Hidalgo-Alvarez, *Journal of colloid and interface science*, 1996, **184**, 259-267.
39. G. Fritz, V. Schädler, N. Willenbacher and N. J. Wagner, *Langmuir*, 2002, **18**, 6381-6390.
40. M. Brynda, T. A. Wesolowski and K. Wojciechowski, *The Journal of Physical Chemistry A*, 2004, **108**, 5091-5099.
41. S. Kong, Y. Wang, H. Zhan, S. Yuan, M. Yu and M. Liu, *Water Environment Research*, 2014, **86**, 147-155.
42. A. A. Ahribesh, S. Lazarević, B. Potkonjak, A. Bjelajac, D. Janaćković and R. Petrović, *Chemical Industry/Hemijska Industrija*, 2015, **69**.
43. Z. Pan, W. Li, J. D. Fortner and D. E. Giammar, *Environmental Science & Technology*, 2017, **51**, 9219-9226.
44. Z. Pan, X. Zhu, A. Satpathy, W. Li, J. D. Fortner and D. E. Giammar, *Environmental science & technology*, 2019, **53**, 11913-11921.
45. A. M. E. Badawy, T. P. Luxton, R. G. Silva, K. G. Scheckel, M. T. Suidan and T. M. Tolaymat, *Environmental science & technology*, 2010, **44**, 1260-1266.
46. H. Zeng, B. Fisher and D. E. Giammar, *Environmental science & technology*, 2008, **42**, 147-152.
47. S. Khaodhiar, M. F. Azizian, K. Osathaphan and P. O. Nelson, *Water, air, and soil pollution*, 2000, **119**, 105-120.
48. J. Bellot and J. Condoret, *Journal of Chromatography A*, 1993, **657**, 305-326.
49. M. Gifford, K. Hristovski and P. Westerhoff, *Science of the Total Environment*, 2017, **601**, 1008-1014.
50. W. Cheng, C. Ding, X. Wang, Z. Wu, Y. Sun, S. Yu, T. Hayat and X. Wang, *Chemical Engineering Journal*, 2016, **293**, 311-318.
51. A. Quintáns-Fondo, G. Ferreira-Coelho, R. Paradelo-Núñez, J. C. Nóvoa-Muñoz, M. Arias-Estévez, M. J. Fernández-Sanjurjo, E. Álvarez-Rodríguez and A. Núñez-Delgado, *Environmental Science and Pollution Research*, 2016, **23**, 19182-19192.
52. S. Minko, in *Polymer surfaces and interfaces*, Springer, 2008, pp. 215-234.
53. C. Steinem and A. Janshoff, *Piezoelectric sensors*, Springer Science & Business Media, 2007.
54. G. Liu and G. Zhang, *QCM-D studies on polymer behavior at interfaces*, Springer, 2013.
55. K. An, M. Park, J. H. Yu, H. B. Na, N. Lee, J. Park, S. H. Choi, I. C. Song, W. K. Moon and T. Hyeon, *Eur J Inorg Chem*, 2012, DOI: DOI 10.1002/ejic.201101193, 2148-2155.
56. R. A. Sperling and W. Parak, *Philosophical Transactions of the Royal Society of London A: Mathematical, Physical and Engineering Sciences*, 2010, **368**, 1333-1383.
57. A. Prakash, H. Zhu, C. J. Jones, D. N. Benoit, A. Z. Ellsworth, E. L. Bryant and V. L. Colvin, *Acs Nano*, 2009, **3**, 2139-2146.
58. E. Vigneau, C. Loisel, M. Devaux and P. Cantoni, *Powder Technology*, 2000, **107**, 243-250.
59. M. C. Dixon, *J Biomol Tech*, 2008, **19**, 151-158.
60. M. Rodahl, F. Höök, A. Krozer, P. Brzezinski and B. Kasemo, *Review of Scientific Instruments*, 1995, **66**, 3924-3930.